

Multiclass threshold-based classification and model evaluation

Edoardo Legnaro

Department of Mathematics (DIMA), University of Genova, Genova, Italy
`edoardo.legnaro@edu.unige.it`

Sabrina Guastavino

Department of Mathematics (DIMA), University of Genova, Genova, Italy
`sabrina.guastavino@unige.it`

Francesco Marchetti

Department of Mathematics “Tullio Levi-Civita”, University of Padova, Padova, Italy
`francesco.marchetti@unipd.it`

December 1, 2025

Abstract

In this paper, we introduce a threshold-based framework for multiclass classification that generalizes the standard argmax rule. This is done by replacing the probabilistic interpretation of softmax outputs with a geometric one on the multidimensional simplex, where the classification depends on a multidimensional threshold. This change of perspective enables for any trained classification network an *a posteriori* optimization of the classification score by means of threshold tuning, as usually carried out in the binary setting, thus allowing for a further refinement of the prediction capability of any network. Our experiments show indeed that multidimensional threshold tuning yields performance improvements across various networks and datasets. Moreover, we derive a multiclass ROC analysis based on *ROC clouds*—the attainable (FPR, TPR) operating points induced by a single multiclass threshold—and summarize them via a *Distance From Point* (DFP) score to $(0, 1)$. This yields a coherent alternative to standard One-vs-Rest (OvR) curves and aligns with the observed tuning gains.

Keywords: multiclass classification, threshold tuning, simplex geometry, ROC, deep learning

MSC codes: 62H30, 68T05, 65K10

1 Introduction

In the standard supervised classification setting, a fundamental distinction is made between the binary and multiclass framework. Although some machine learning methods are natively binary, in deep learning this distinction leads to two different types of output of the neural network, which are handled differently in order to get predictions and then performance assessment [7, 36].

1.1 The binary case

In the binary classification setting, each element \mathbf{x}_i of the d -dimensional dataset $\mathcal{X} = \{\mathbf{x}_1, \dots, \mathbf{x}_n\} \subset \Omega \subset \mathbb{R}^d$ is associated with a label $y_i \in \{0, 1\}$. The aim is to learn the sample-label association by means of a network that produces the output

$$\hat{y}_{\boldsymbol{\theta}}(\mathbf{x}) = (\sigma \circ h)(\mathbf{x}, \boldsymbol{\theta}) \in [0, 1], \quad \mathbf{x} \in \Omega,$$

where $h(\mathbf{x}, \boldsymbol{\theta})$ denotes the outcome of the *input* and *hidden* layers, which depend on a vector (matrix) of weight parameters $\boldsymbol{\theta}$, and σ is the well-known *sigmoid* activation function defined as $\sigma(h) = (1 + e^{-h})^{-1}$.

Then, the classification of a sample \mathbf{x} to one class or the other depends on a threshold, that is, the corresponding output $\hat{y} = \hat{y}_{\boldsymbol{\theta}}(\mathbf{x})$ is assigned to one of the two labels $\{y = 0\}$ or $\{y = 1\}$ by means of a function:

$$\mathbb{1}_{\hat{y}}(\tau) = \mathbb{1}_{\{\hat{y} > \tau\}} = \begin{cases} 0 & \text{if } \hat{y} \leq \tau, \\ 1 & \text{if } \hat{y} > \tau, \end{cases}$$

being $\tau \in (0, 1)$ a threshold value.

Once the network is trained by minimizing some objective function, the performance of the model is usually assessed by means of some classification score s , which is a function that takes input from the entries of the confusion matrix:

$$\text{CM}(\tau, \boldsymbol{\theta}) = \begin{pmatrix} \text{TN}(\tau, \boldsymbol{\theta}) & \text{FP}(\tau, \boldsymbol{\theta}) \\ \text{FN}(\tau, \boldsymbol{\theta}) & \text{TP}(\tau, \boldsymbol{\theta}) \end{pmatrix}, \quad (1)$$

being

$$\begin{aligned} \text{TN}(\tau, \boldsymbol{\theta}) &= \sum_{i=1}^n (1 - y_i) \mathbb{1}_{\{\hat{y}_{\boldsymbol{\theta}}(\mathbf{x}_i) < \tau\}}, & \text{TP}(\tau, \boldsymbol{\theta}) &= \sum_{i=1}^n y_i \mathbb{1}_{\{\hat{y}_{\boldsymbol{\theta}}(\mathbf{x}_i) > \tau\}}, \\ \text{FP}(\tau, \boldsymbol{\theta}) &= \sum_{i=1}^n (1 - y_i) \mathbb{1}_{\{\hat{y}_{\boldsymbol{\theta}}(\mathbf{x}_i) > \tau\}}, & \text{FN}(\tau, \boldsymbol{\theta}) &= \sum_{i=1}^n y_i \mathbb{1}_{\{\hat{y}_{\boldsymbol{\theta}}(\mathbf{x}_i) < \tau\}}. \end{aligned} \quad (2)$$

We note that a meaningful score is not decreasing with respect to TN and TP and is not increasing with respect to FN and FP. The reliance on a threshold has allowed the development of a straightforward solution for *a posteriori* score optimization, that is, once the network is trained and the *optimal* weights $\boldsymbol{\theta}^*$ are defined, find the threshold value that maximizes your classification metric of interest

$$\max_{\tau \in (0, 1)} s(\text{CM}(\tau, \boldsymbol{\theta}^*)). \quad (3)$$

This tuning, which is performed using the training or validation set, can severely improve the performance of the network, especially when settings with unbalanced classes are considered, and it represents a common practice in this framework. We also recall that, in the binary setting, *score-oriented loss* functions have been proposed to incorporate the desired evaluation metric directly into the training objective via probabilistic confusion matrices [19].

In addition or alternatively to threshold tuning, classifier performance can be evaluated across all possible thresholds, which is the main principle underpinning the well-known Receiver Operating Characteristic (ROC) analysis. In particular, the ROC curve plots the true positive rate (TPR, or sensitivity) against the false positive rate (FPR, or 1-specificity) as the decision threshold is varied [5]. Here, TPR is defined as the proportion of correctly identified positive samples, while FPR is the proportion of negative samples incorrectly classified as positive. This graphical approach provides a comprehensive view of a model's discriminative ability, independent of any specific threshold choice. To summarize the information provided by the ROC curve, the area under the curve (AUC) is often reported and can be interpreted as the probability that a randomly chosen positive instance is ranked higher than a randomly chosen negative instance [2]. Precisely, an AUC of 1 indicates perfect classification, while an AUC of 0.5 corresponds to random guessing, which corresponds to the case where the ROC curve is the diagonal bisector line. ROC and AUC are thus standard tools for comparing classifiers, especially in imbalanced or cost-sensitive scenarios.

1.2 The multiclass case

In contrast to the binary setting, when approaching a multiclass problem where C_1, \dots, C_m are $m > 2$ classes and each $y_i \in C_j$ for a unique $j = 1, \dots, m$, the classification is no longer based on a threshold value. Instead, σ is a *softmax* activation function, which models the output as

$$\hat{y}_{\theta} = (\hat{y}_{\theta}^1, \dots, \hat{y}_{\theta}^m), \quad \sum_{j=1}^m \hat{y}_{\theta}^j = 1.$$

Then, a sample x is usually assigned to the class j^* that represents the *argmax* of \hat{y}_{θ} with respect to the m classes, that is, the output is interpreted as a probability distribution and [22]

$$j^* = \operatorname{argmax}_{j=1, \dots, m} \hat{y}_{\theta}^j.$$

Although a single sigmoid unit is usually chosen because of its simpler implementation and interpretation, we point out that two softmax units can be used in the binary framework. In this case, the value of one unit is redundant, and the argmax rule plays the role of a 0.5 threshold value.

Alternative prediction rules to the standard argmax have been explored in several works on multiclass classification [3, 20]. For example, in [24] the replacement of the argmax with the Fréchet mean was proposed, which enables pre-trained models to generalize to novel classes by leveraging the geometric structure of the label space, without requiring additional training. More recently, [26] introduced a stable relaxation of the argmax, termed the “inflated argmax”, with the objective of improving the stability of multiclass classifiers.

In the multiclass scenario, the classification results are very often evaluated in terms of an extension of the binary score to the multiclass case, which is computed by considering m *one-vs-rest* (OvR) confusion matrices (1), where a class is considered positive and the set of remaining ones as negative. However, in this manner, a posteriori score optimization cannot be performed via some threshold variation if an argmax-like classification rule is applied, or at least there is no native way to do so. To obtain some a posteriori improvement in the classification performance, another strategy is represented by the so-called model calibration, whose goal is to postprocess a model’s scores so that they better align with true class probabilities. This is typically achieved by training a secondary model, such as a Platt scaler or an isotonic regressor, on the outputs of a pre-trained classifier [9]. In fact, since they deal with OvR-computed scores, well-established standard multiclass calibration techniques are extensions of binary methods and often rely on an OvR decomposition [35], where a separate calibrator is trained for each class, thus losing the original intertwined structure of the multiclass network output. Analogous issues affect ROC analysis in the presence of more than two classes. In fact, the OvR approach yields to multiple ROC curves, one for each class [10], which are then aggregated using macro-averaged or weighted-averaged AUC scores. However, simply averaging summarizing scalar metrics could lead to oversimplification, and, in a sense that will be deepened in 4, such a procedure relies on decision rules that are *unnatural* for the multiclass framework. These approaches fall largely into two main categories: those that extend decomposition strategies and those that attempt a more direct geometric generalization. Another influential decomposition strategy is the One-vs-One (OvO) approach, which trains a unique binary classifier for every pair of classes [1, 30]. For a problem with K classes, this results in $K(K - 1)/2$ classifiers [30]. In [10] a multiclass AUC measure was proposed, now commonly known as MAUC, based on this principle by averaging the AUCs of all pairwise comparisons. The second major branch of research pursues a more theoretically direct generalization by defining a high-dimensional ROC “hypersurface” [13, 30]. In this framework, the performance of a classifier is summarized by Volume Under the Surface (VUS) or Hypervolume Under the Manifold (HUM) [6, 17, 16].

1.3 Our contribution

In this paper, our aim is to provide a novel framework by introducing a threshold-based setting for the multiclass case that generalizes the classical argmax operation. This is obtained by discarding the probabilistic interpretation of the softmax-based output and considering it in its natural domain, which is the multidimensional simplex [27]. We observe that simplex geometry has previously been used for multiclass classification in various approaches for different purposes. In [21], the classification task is reformulated as a vector-valued regression problem, where the model learns to map inputs to points in a regular simplex, allowing for a geometrically structured representation of class labels. In [12], the simplex is instead utilized in the latent space: the training data is embedded in a space whose geometry is defined by a regular $(m - 1)$ -dimensional simplex, with m denoting the number of classes.

By considering the output vector as a single point in the simplex, our method offers a natively multiclass framework that preserves the relationships between all class scores simultaneously. The novelty of our approach lies in performing classification by relating each class to a corresponding subset of the simplex, thanks to the introduction of a multidimensional threshold parameter, which allows for

- a native *a posteriori* optimization of a score, which can be easily applied to any trained network, as in the binary setting;
- a consequent *coherent* ROC analysis, which is aligned with the multiclass network output, differently with respect to the standard strategies such as OvR or OvO.

We point out that our approach, despite operating on the model’s output, is conceptually distinct from calibration methods, being an inference-time decision rule that operates directly on the raw, uncalibrated output vector provided by the softmax function, and requires no additional training or post-hoc model fitting.

Building on the simplex decision rule, we introduce *ROC clouds* for multiclass models: for each multidimensional threshold in the simplex, we obtain a coherent, natively multiclass operating point that yields classwise (FPR, TPR) pairs. Varying the threshold generates, for each class, a point cloud in the ROC plane that reflects global, joint trade-offs under a single decision rule. We summarize each cloud with a *Distance From Point* (DFP) score—the mean L_1 distance to $(0, 1)$ over sampled thresholds—which provides a compact, threshold-agnostic evaluation aligned with our tuning framework.

The paper is organized as follows. In 2, we formalize our novel threshold-based framework, from which we derive the threshold tuning algorithm in 3. This allows for a linked multiclass ROC analysis, which is described in detail and compared to the standard approach in 4. The results presented in 5 show that multidimensional threshold tuning is effective in improving the classification performance obtained by means of the classical argmax rule.

2 Predicting in the multidimensional simplex

In this section, our purpose is to show that a threshold-based framework can be recovered in the multiclass setting too, allowing an improved flexible handling of the output with the aim of then enhancing score performance and model analysis. To provide a clear setting and subsequent, we will explicitly formalize some crucial concepts.

First, we observe that the output $\hat{\mathbf{y}}$ is contained in the $(m - 1)$ -simplex $S_m = \{\mathbf{z} \in \mathbb{R}^m \mid \sum_{j=1}^m \mathbf{z}^j = 1\}$, whose vertices are the *one-hot* encoded classes $\mathbf{e}_1, \dots, \mathbf{e}_m$ corresponding to C_1, \dots, C_m [11]. Then, we provide the following definition.

Definition 1 (Simplex classification collection). *Let $\boldsymbol{\tau} = (\tau^1, \dots, \tau^m) \in S_m$ be a multidimensional threshold. A simplex classification collection $R_1(\boldsymbol{\tau}), \dots, R_m(\boldsymbol{\tau})$ of classification regions $R_j(\boldsymbol{\tau})$ for the class C_j , $j = 1, \dots, m$, satisfies the following properties.*

1. $R_j(\boldsymbol{\tau}) \subset S_m$ for $j = 1, \dots, m$,
2. $e_j \in R_j(\boldsymbol{\tau})$ for $j = 1, \dots, m$,
3. $cl(\bigcup_{j=1}^m R_j(\boldsymbol{\tau})) = S_m$,

being cl the topological closure.

According to 1, any point in the simplex is assigned to at least one classification region $R_1(\boldsymbol{\tau}), \dots, R_m(\boldsymbol{\tau})$, but a set of points that lie in subsets of S_m of null measure. This ambiguity is actually present in classical binary and multiclass classification. For example, in an argmax-driven 3-class problem, the output $(0.5, 0.5, 0)$ is in principle undecided between the first and the second class.

Another critical point in 1 is the fact that one output in the simplex could be assigned to more than one class. In 4, we will discuss in which way this is connected to classical ROC analysis, but with the following definition we restrict ourselves to simplex classification collections that are not affected by this multilabel temptation.

Definition 2 (Proper simplex classification collection). *Let $\boldsymbol{\tau} = (\tau^1, \dots, \tau^m) \in S_m$ be a multidimensional threshold. A simplex classification collection $R_1(\boldsymbol{\tau}), \dots, R_m(\boldsymbol{\tau})$ is called proper if*

$$R_k(\boldsymbol{\tau}) \cap R_j(\boldsymbol{\tau}) = \emptyset$$

for $k, j = 1, \dots, m$, $k \neq j$.

Therefore, a proper classification collection consists of a sort of partition of the simplex S_m , where each output is now assigned to one class, besides null measure subsets, which is a crucial aspect to get a well-posed classification scheme. In particular, note that varying $\boldsymbol{\tau}$ will produce a variation in the corresponding *classification rule*, i.e., the procedure that assigns a class to the received output.

Among the possible classification collections that can be defined in the simplex, in the following we consider classification regions defined as

$$R_j(\boldsymbol{\tau}) = \{\mathbf{z} \in S_m \mid z^j - z^k > \tau^j - \tau^k, k \neq j\}, \quad j = 1, \dots, m. \quad (4)$$

We will refer to this choice as the *natural* classification collection, as we motivate in the following proposition.

Proposition 1. *The simplex classification collection defined in (4) is proper and generalizes the argmax procedure, i.e., the classical argmax is a particular case of (4).*

Proof. The collection is trivially proper, because $\mathbf{z} \in R_k(\boldsymbol{\tau}) \cap R_j(\boldsymbol{\tau})$, $k \neq j$, would imply both $z^j > z^k$ and $z^k > z^j$. Then, if $\tau^j = 1/m$ for any $j = 1, \dots, m$, then $R_j(\boldsymbol{\tau}) = \{\mathbf{z} \in S_m \mid z^j > z^k, k \neq j\}$ leads to the classical argmax procedure. \square

See 1 for examples of natural classification collections obtained by varying the threshold vector.

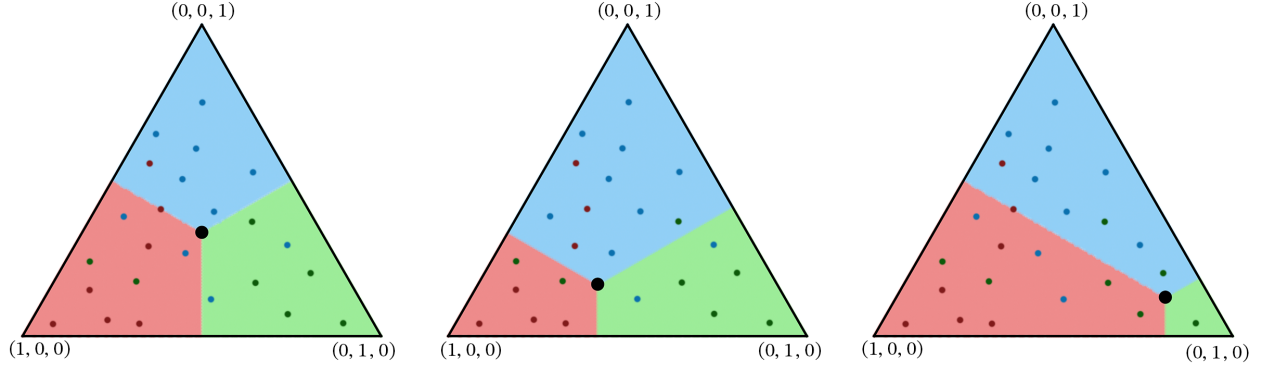


Figure 1: For $m = 3$, the three regions $R_1(\boldsymbol{\tau})$ (red), $R_2(\boldsymbol{\tau})$ (green) and $R_3(\boldsymbol{\tau})$ (blue). From left to right: $\boldsymbol{\tau} = (1/3, 1/3, 1/3)$, $\boldsymbol{\tau} = (1/2, 1/3, 1/6)$, $\boldsymbol{\tau} = (1/8, 3/4, 1/8)$ (big black dot). The color blue, red or green represents the true label of the samples (colored dots). Number of misclassifications from left to right: 7, 8 and 10.

3 Multiclass threshold-based optimization

The threshold-based framework introduced in the previous section can be used to obtain an *optimized* multiclass classification rule by performing a posteriori threshold tuning, analogously to the binary case.

Letting s be a binary score, for each $j = 1, \dots, m$ we can consider

$$\text{CM}_j(\boldsymbol{\tau}, \boldsymbol{\theta}) = \begin{pmatrix} \text{TN}_j(\boldsymbol{\tau}, \boldsymbol{\theta}) & \text{FP}_j(\boldsymbol{\tau}, \boldsymbol{\theta}) \\ \text{FN}_j(\boldsymbol{\tau}, \boldsymbol{\theta}) & \text{TP}_j(\boldsymbol{\tau}, \boldsymbol{\theta}) \end{pmatrix},$$

with

$$\begin{aligned} \text{TN}_j(\boldsymbol{\tau}, \boldsymbol{\theta}) &= \sum_{i=1}^n \mathbb{1}_{\{\mathbf{y}_i \neq \mathbf{e}_j\}} \mathbb{1}_{\{\hat{\mathbf{y}}_{\boldsymbol{\theta}}(\mathbf{x}_i) \notin R_j(\boldsymbol{\tau})\}}, & \text{TP}_j(\boldsymbol{\tau}, \boldsymbol{\theta}) &= \sum_{i=1}^n \mathbb{1}_{\{\mathbf{y}_i = \mathbf{e}_j\}} \mathbb{1}_{\{\hat{\mathbf{y}}_{\boldsymbol{\theta}}(\mathbf{x}_i) \in R_j(\boldsymbol{\tau})\}}, \\ \text{FP}_j(\boldsymbol{\tau}, \boldsymbol{\theta}) &= \sum_{i=1}^n \mathbb{1}_{\{\mathbf{y}_i \neq \mathbf{e}_j\}} \mathbb{1}_{\{\hat{\mathbf{y}}_{\boldsymbol{\theta}}(\mathbf{x}_i) \in R_j(\boldsymbol{\tau})\}}, & \text{FN}_j(\boldsymbol{\tau}, \boldsymbol{\theta}) &= \sum_{i=1}^n \mathbb{1}_{\{\mathbf{y}_i = \mathbf{e}_j\}} \mathbb{1}_{\{\hat{\mathbf{y}}_{\boldsymbol{\theta}}(\mathbf{x}_i) \notin R_j(\boldsymbol{\tau})\}}. \end{aligned}$$

Note that $\hat{\mathbf{y}}$ is assigned to the positive class for a unique CM_j only, being negative in the other confusion matrices corresponding to different indices.

Then, the contribution of all confusion matrices can be combined in a vector

$$\mathbf{s}(\boldsymbol{\tau}, \boldsymbol{\theta}) = (s(\text{CM}_1(\boldsymbol{\tau}, \boldsymbol{\theta})), \dots, s(\text{CM}_m(\boldsymbol{\tau}, \boldsymbol{\theta}))), \quad (5)$$

and summarized by taking, e.g., the mean value

$$s_{\text{mean}}(\boldsymbol{\tau}, \boldsymbol{\theta}) = \frac{1}{m} \|\mathbf{s}(\boldsymbol{\tau}, \boldsymbol{\theta})\|_1.$$

Averaging over the contributions of all binary scores, as considered here, is the so-called *macro* setting, which is particularly useful in presence of unbalancing in classes' distribution. Then, a posteriori maximization can be carried out after the training phase by computing (cf. (3))

$$\max_{\boldsymbol{\tau} \in S_m} s_{\text{mean}}(\boldsymbol{\tau}, \boldsymbol{\theta}^*). \quad (6)$$

We sum up our score maximization scheme in Algorithm 1, and in 5 we present several classification tests that show the effectiveness of the algorithm in improving the performance of trained networks.

Algorithm 1 Multidimensional threshold tuning

- 1: **Input:** True labels $\{\mathbf{y}_1, \dots, \mathbf{y}_n\}$, corresponding predictions from trained network $\{\hat{\mathbf{y}}_{\boldsymbol{\theta}^*}(\mathbf{x}_1), \dots, \hat{\mathbf{y}}_{\boldsymbol{\theta}^*}(\mathbf{x}_n)\}$ (training or validation set), classification score s
- 2: **Output:** Best threshold $\boldsymbol{\tau}^*$
- 3: Sample $\boldsymbol{\tau}_1, \dots, \boldsymbol{\tau}_M$ threshold values on the simplex S_m (e.g. uniform grid)
- 4: **for** $k = 1, \dots, M$ **do**
- 5: Construct $\text{CM}_j(\boldsymbol{\tau}_k, \boldsymbol{\theta}^*)$ for each $j = 1, \dots, m$
- 6: Evaluate $s(\text{CM}_j(\boldsymbol{\tau}_k, \boldsymbol{\theta}^*))$ for each $j = 1, \dots, m$
- 7: Calculate $s_{\text{mean}}(\boldsymbol{\tau}_k, \boldsymbol{\theta}^*) = \frac{1}{m} \sum_{j=1}^m s(\text{CM}_j(\boldsymbol{\tau}_k, \boldsymbol{\theta}^*))$
- 8: **end for**
- 9: Compute $\boldsymbol{\tau}^* = \boldsymbol{\tau}_{k^*}$ where $k^* = \text{argmax}_{k=1, \dots, M} s_{\text{mean}}(\boldsymbol{\tau}_k, \boldsymbol{\theta}^*)$

4 ROC analysis in the simplex

When dealing with multiple classes in the ROC analysis, the classical approach consists of building many ROC curves, one for each class considered positive *versus* the other classes considered negative, which may be then aggregated a posteriori to summarize the overall performance of the classifier. Formally, this approach can be formalized as follows. For each class $i = 1, \dots, m$, the multiclass output is binarized as

$$\hat{\mathbf{y}}_{\boldsymbol{\theta}} = (\hat{y}_{\boldsymbol{\theta}}^1, \dots, \hat{y}_{\boldsymbol{\theta}}^m) \implies \hat{\mathbf{y}}_{\boldsymbol{\theta},i} = \left(\hat{y}_{\boldsymbol{\theta}}^i, \sum_{j \neq i} \hat{y}_{\boldsymbol{\theta}}^j \right),$$

so that the native binary procedure can be applied separately for each $\hat{\mathbf{y}}_{\boldsymbol{\theta},i}$, $i = 1, \dots, m$.

To better understand the discrepancy that this OvR approach determines with respect to the true multiclass output offered by the classifier, we can take advantage of our simplex framework. In fact, in S_m , this is equivalent to considering the classification collection produced by the following classification regions:

$$\bar{R}_j(\boldsymbol{\tau}) = \{\mathbf{z} \in S_m \mid z^j > \tau^j\}, \quad j = 1, \dots, m.$$

Note that the collection $\bar{R}_1(\boldsymbol{\tau}), \dots, \bar{R}_m(\boldsymbol{\tau})$ satisfies in fact the requirements of Definition 1, but it is not proper according to Definition 2, as $\bar{R}_i(\boldsymbol{\tau}) \cap \bar{R}_j(\boldsymbol{\tau}) \neq \emptyset$ for $i, j = 1, \dots, m$ (see 2 and cf. 1). Therefore, the major flaws of this approach are:

- Each classification region does not relate to the others, completely ignoring the information provided by the classifier that *jointly* distinguish among multiple classes, leading to its incomplete evaluation.
- Since the collection is not proper, we are formally considering a hybrid multiclass-multilabel framework, where an element might belong to more than one class, which substantially differs with respect to the classification process carried out in the training phase.

Thanks to our threshold-based framework, fixed a score s and with the choice (4), we recall that we can construct m classification matrices for a fixed threshold value $\boldsymbol{\tau} \in S_m$, and derive a vector \mathbf{s} of corresponding score values (see (5)). Therefore, focusing on FPR and TPR scores, we can obtain a map

$$\boldsymbol{\tau} \longrightarrow \{fpr(\boldsymbol{\tau}), tpr(\boldsymbol{\tau})\}, \tag{7}$$

where we omitted the dependence on the weights of the network.

To clarify this procedure with an example, let us again consider the setting in 1.

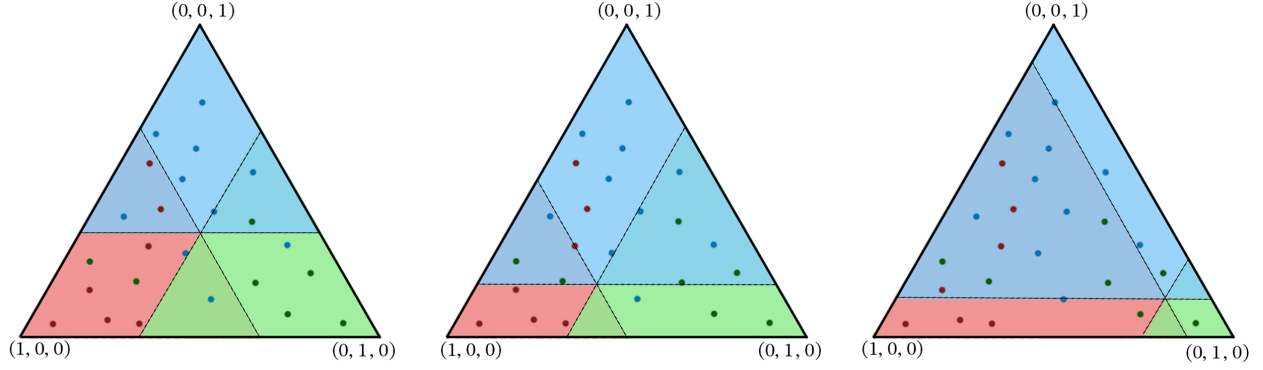


Figure 2: For $m = 3$, the three regions $\bar{R}_1(\tau)$ (red), $\bar{R}_2(\tau)$ (green) and $\bar{R}_3(\tau)$ (blue). From left to right: $\tau = (1/3, 1/3, 1/3)$, $\tau = (1/2, 1/3, 1/6)$, $\tau = (1/8, 3/4, 1/8)$ (big black dot). Differently with respect to 1, here each region is unrelated to the others and overlapping is allowed.

- For $\tau = (1/3, 1/3, 1/3)$, we get $fpr(\tau) = (4/17, 2/17, 1/14)$ and $tpr(\tau) = (6/7, 5/7, 6/10)$.
- For $\tau = (1/2, 1/3, 1/6)$, we have $fpr(\tau) = (2/17, 2/17, 4/14)$ and $tpr(\tau) = (4/7, 4/7, 8/10)$.
- For $\tau = (1/8, 3/4, 1/8)$, we get $fpr(\tau) = (7/17, 0, 3/14)$ and $tpr(\tau) = (6/7, 1/7, 7/10)$.

By computing the scores for many threshold values τ_1, \dots, τ_M , we can obtain multiple sets

$$\{fpr(\tau_1), tpr(\tau_1)\}, \dots, \{fpr(\tau_M), tpr(\tau_M)\}. \quad (8)$$

Now, we need to process (8) to extract information on the performance of the classifier. Fixed τ_k , each couple $fpr(\tau_k), tpr(\tau_k)$ might be framed in $[0, 1]^m \times [0, 1]^m$ space. Consequently, by varying τ across the simplex and in light of (7), one could interpret (8) as a set of achievable points that form a surface in the reference space. However, this surface can not be directly visualized for $m > 3$, and interpreting its properties for model evaluation purposes is an intricate task. Alternatively, we reduce our setting to 2D *projections*, that is, we collect the i -th coordinates of each vector to determine 2D points as

$$(fpr^j(\tau_1), tpr^j(\tau_1)), \dots, (fpr^j(\tau_M), tpr^j(\tau_M)),$$

and thus define for each $j = 1, \dots, m$ a ROC cloud in the usual FPR/TPR plane. Then, the information can be summarized by considering the following Distance From Point (DFP) measure:

$$DFP_j = \frac{1}{M} \sum_{k=1}^M \|(fpr^j(\tau_k), tpr^j(\tau_k)) - (0, 1)\|_1, \quad j = 1, \dots, m, \quad (9)$$

being $(0, 1)$ the FPR/TPR output of a perfect classification, and the metrics of all classes can be combined in a unique DFP measure by taking, e.g., the mean value; see Algorithm 2 for a formalization of the proposed procedure.

Note that each DFP_j consists of a discrete L_1 -Wasserstein distance, that is, the transport measure that computes the mean value of the L_1 distances covered to move the FPR/TPR couples onto the $(0, 1)$ point. The choice for the L_1 distance, also called the Manhattan distance, is motivated by the fact that the FPR/TPR couples lying in the *random bisector* of the ROC plane

Algorithm 2 ROC analysis in the multidimensional simplex

- 1: **Input:** True labels $\{\mathbf{y}_1, \dots, \mathbf{y}_n\}$, corresponding predictions from trained network $\{\hat{\mathbf{y}}_{\theta^*}(\mathbf{x}_1), \dots, \hat{\mathbf{y}}_{\theta^*}(\mathbf{x}_n)\}$ (training or validation set)
- 2: **Output:** ROC clouds, ROC-DFP measure
- 3: Sample $\boldsymbol{\tau}_1, \dots, \boldsymbol{\tau}_M$ threshold values on the simplex S_m (e.g. uniform grid)
- 4: **for** $k = 1, \dots, M$ **do**
- 5: Calculate the vectors $fpr(\boldsymbol{\tau}_k), tpr(\boldsymbol{\tau}_k)$
- 6: **end for**
- 7: **for** $j = 1, \dots, m$ **do**
- 8: Set the ROC cloud $(fpr^j(\boldsymbol{\tau}_1), tpr^j(\boldsymbol{\tau}_1)), \dots, (fpr^j(\boldsymbol{\tau}_M), tpr^j(\boldsymbol{\tau}_M))$
- 9: Compute the measure DFP_j as in (9)
- 10: **end for**
- 11: Calculate the summarizing $DFP = \frac{1}{m} \sum_{j=1}^m DFP_j$

are then equidistant from $(0, 1)$ and at maximum distance. Consequently, while $DFP_j = 0$ is the perfect result, $DFP_j = 1$ is the maximum value in a random setting.

We remark that the crucial difference of our approach from the classical one is that here the FPR/TPR couples that lean the ROC analysis are not the result of separate threshold evaluations but are intertwined among the classes, as they rely on the same multidimensional threshold value, being natively multiclass and more coherent with the actual output of the multiclass model; see 1.

	Classical	Our approach
Threshold(s)	Separate independent thresholds for each class	Unique multidimensional threshold for all classes
Outputs	Unrelated FPR/TPR OvR couples	Intertwined FPR/TPR OvR couples
Analysis tool	OvR ROC curves	OvR ROC clouds
Summary metric	AUC	DFP

Table 1: Key differences between the classical multidimensional ROC analysis and our proposed approach in the threshold-based framework in the simplex.

5 Results

The experiments for this project can be run on consumer-grade hardware. In our case, they were conducted on a desktop PC equipped with 64 GB of RAM, a 16-core AMD Ryzen 5950X CPU, and an NVIDIA RTX 3070 GPU with 8 GB of VRAM.

The threshold tuning python package is available at

<https://github.com/edoardolegnaro/SimplexTools>.

5.1 Multiclass threshold optimization

In this subsection, our purpose is to show the effectiveness of the proposed threshold tuning approach (see Algorithm 1) in refining the performance of a classifier trained with the weighted

Dataset	Class	Train	Validation	Test
SOLAR-STORM1	α	3821 (33.01%)	888 (30.68%)	567 (48.38%)
	β	5691 (49.17%)	1662 (57.43%)	496 (42.32%)
	βX	2063 (17.82%)	344 (11.89%)	109 (9.30%)
Total		11575	2894	1172
OCTMNIST	choroidal neovascularization	33484 (34.35%)	3721 (34.35%)	250 (25.00%)
	diabetic macular edema	10213 (10.48%)	1135 (10.48%)	250 (25.00%)
	drusen	7754 (7.95%)	862 (7.96%)	250 (25.00%)
	normal	46026 (47.22%)	5114 (47.21%)	250 (25.00%)
Total		97477	10832	1000
PATHMNIST	adipose	9366 (10.41%)	1041 (10.41%)	1338 (18.64%)
	background	9509 (10.57%)	1057 (10.57%)	847 (11.80%)
	debris	10360 (11.51%)	1152 (11.52%)	339 (4.72%)
	lymphocytes	10401 (11.56%)	1156 (11.56%)	634 (8.83%)
	mucus	8006 (8.90%)	890 (8.90%)	1035 (14.42%)
	smooth muscle	12182 (13.54%)	1354 (13.53%)	592 (8.25%)
	normal colon mucosa	7886 (8.76%)	877 (8.77%)	741 (10.32%)
	cancer-associated stroma	9401 (10.45%)	1045 (10.45%)	421 (5.86%)
	colorectal adenocarcinoma epithelium	12885 (14.32%)	1432 (14.31%)	1233 (17.17%)
Total		89996	10004	7180
FASHIONMNIST	T-shirt/top	4836 (10.08%)	1210 (10.08%)	1000 (10.00%)
	Trouser	4812 (10.03%)	1264 (10.53%)	1000 (10.00%)
	Pullover	4773 (9.94%)	1207 (10.06%)	1000 (10.00%)
	Dress	4774 (9.95%)	1146 (9.55%)	1000 (10.00%)
	Coat	4800 (10.00%)	1243 (10.36%)	1000 (10.00%)
	Sandal	4833 (10.07%)	1180 (9.83%)	1000 (10.00%)
	Shirt	4867 (10.14%)	1183 (9.86%)	1000 (10.00%)
	Sneaker	4786 (9.97%)	1176 (9.80%)	1000 (10.00%)
	Bag	4749 (9.89%)	1194 (9.95%)	1000 (10.00%)
	Ankle boot	4770 (9.94%)	1197 (9.98%)	1000 (10.00%)
Total		48000	12000	10000

Table 2: Classes distributions for SOLAR-STORM1, OCTMNIST, PATHMNIST, and FASHIONMNIST datasets.

categorical CE. Different datasets with varying numbers of labels m are considered. The distributions of the classes over training, validation and test sets for the datasets are provided in 2. First, we consider the task of classifying solar active regions (ARs) into their magnetic type [8]. We take the SOLAR-STORM1 dataset provided in [4], which consists of images of sunspots from the Helioseismic and Magnetic Imager (HMI) instrument on Solar Dynamics Observatory (SDO) satellite [23, 25]. The classes are three: α (unipolar sunspots), β (bipolar sunspots) and βX (complex sunspots), with unbalanced classes distributions. We consider a Data Efficient Image Transformer (DeiT, [28]) with about 86.6M parameters (the `deit_base_patch16_224` implementation from [31]) trained following [18]. The scores found are reported in 3 (top), and in 3 we show the distribution of the scores obtained by varying the threshold in the 2-simplex.

The remaining experiments in 3 are carried out by training a `resnet18` model, also making use of standard tools such as: data augmentations, mixed precision training, Adam optimizer and an early stopping rule. The network weights are restored to the best validation case in order to make predictions for the test. We show the results obtained for OCTMNIST [15], PATHMNIST

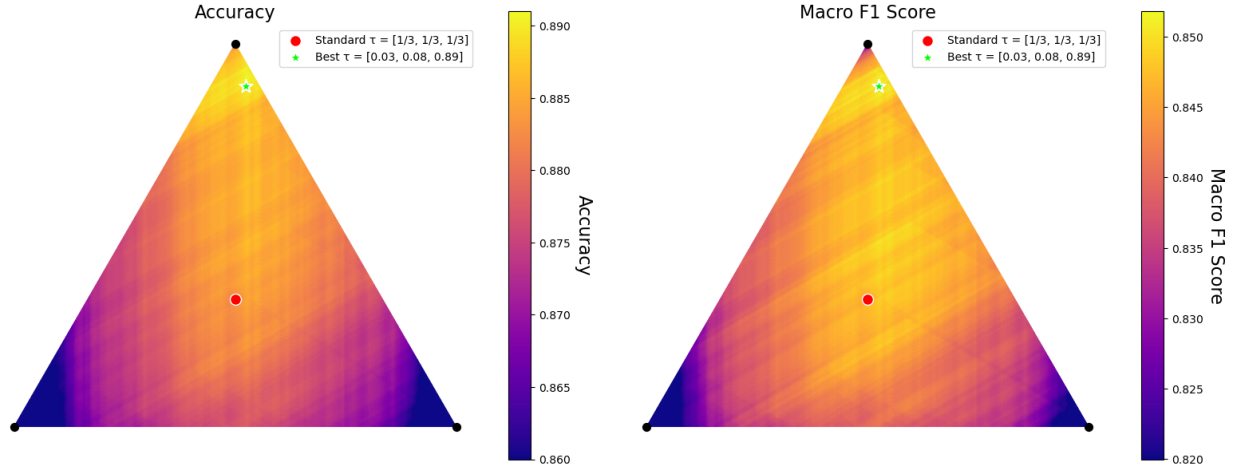


Figure 3: Accuracy (left) and Macro F1 Score (right) heatmaps across the simplex for the validation set. The color intensity represents the metric’s value, with lighter shades indicating higher performance. The standard threshold $\tau = (1/3, 1/3, 1/3)$ is marked with a red circle, while the threshold giving the best score is indicated by a green star, corresponding to $\tau^* = (0.00, 0.06, 0.94)$ for accuracy and $\tau^* = (0.01, 0.08, 0.91)$ for the Macro F1 Score. Here, the grid of evaluation thresholds consists of $M = 20301$ samples.

[14] [33, 34] and FASHIONMNIST [32].

To provide a more comprehensive evaluation, besides the standard *argmax* rule, the performance of the proposed multidimensional threshold tuning (“Tuned”) was benchmarked against two other recently developed decision rules from the literature: the Fréchet mean [24] and the ε -inflated *argmax* [26]. A notable characteristic of the ε -inflated *argmax* is its capacity to predict a set of labels rather than a single classification output. Consequently, its performance was assessed using two specific metrics:

- **Coverage**, which considers a prediction correct if the true label is contained within the predicted set.
- **Singleton**, which calculates accuracy in the conventional manner but is restricted to predictions where the output set consists of a single label.

The experimental results are summarised in 4. As indicated by the “Average Set Size” metric, non-singleton predictions were infrequent in the experiments.

Dataset	Metric	Set	Method	Value	Delta	Validation τ^*
SOLAR-STORM1 ($m = 3$)	Accuracy	Validation	Argmax	0.8829	0.0069	(0.00 0.06 0.94)
			Tuned	0.8898		
	F1 Score	Test	Argmax	0.8831	0.0154	(0.01 0.08 0.91)
			Tuned	0.8985		
OCTMNIST ($m = 4$)	Accuracy	Validation	Argmax	0.8462	0.0041	(0.01 0.08 0.91)
			Tuned	0.8503		
	F1 Score	Test	Argmax	0.8527	0.0252	(0.16 0.24 0.46 0.14)
			Tuned	0.8779		
PATHMNIST ($m = 9$)	Accuracy	Validation	Argmax	0.8816	0.0297	(0.00 0.24 0.64 0.12)
			Tuned	0.9113		
	F1 Score	Test	Argmax	0.8420	0.0000	(0.00 0.56 0.44 0.00 0.00)
			Tuned	0.8420		
FASHIONMNIST ($m = 10$)	Accuracy	Validation	Argmax	0.9705	0.0006	(0.00 0.56 0.44 0.00 0.00)
			Tuned	0.9711		
	F1 Score	Test	Argmax	0.9125	0.0000	(0.00 0.00 0.00 0.00 0.00)
			Tuned	0.9125		
	Accuracy	Validation	Argmax	0.9705	0.0007	(0.00 0.56 0.44 0.00 0.00)
			Tuned	0.9712		
	F1 Score	Test	Argmax	0.8760	0.0016	(0.00 0.00 0.00 0.00 0.00)
			Tuned	0.8776		
	Accuracy	Validation	Argmax	0.9838	0.0004	(0.00 0.67 0.00 0.00 0.33)
			Tuned	0.9842		
	F1 Score	Test	Argmax	0.9347	0.0000	(0.00 0.00 0.00 0.00 0.00)
			Tuned	0.9347		

Table 3: Performance metrics for different datasets with corresponding best validation threshold τ^* .

Dataset	Set	Argmax	Tuned (our)	Fréchet	ε -inflated Argmax		
					Coverage	Singleton	Avg Set Size
SOLAR-STORM1	Validation	0.8829	0.8898	0.8829	0.8856	0.8818	1.0038
	Test	0.8831	0.8985	0.8831	0.8882	0.8805	1.0077
OCTMNIST	Validation	0.8816	0.9093	0.8816	0.8883	0.8744	1.0147
	Test	0.8420	0.8420	0.8420	0.8510	0.8340	1.0170
PATHMNIST	Validation	0.9705	0.9711	0.9705	0.9709	0.9695	1.0020
	Test	0.9125	0.9125	0.9125	0.9149	0.9102	1.0054
FASHIONMNIST	Validation	0.9838	0.9842	0.9809	0.9811	0.9804	1.0008
	Test	0.9347	0.9347	0.9347	0.9361	0.9339	1.0027

Table 4: Comparison of accuracy for different decision rules. For the ε -inflated argmax, “Coverage” indicates correctness if the true label is in the predicted set, while “Singleton” is the accuracy on single-label predictions.

5.2 ROC analysis

To demonstrate the proposed ROC analysis framework, we consider two datasets: SOLAR-STORM1 ($m=3$) and OCTMNIST ($m=4$). On each test set, we vary the multidimensional threshold τ uniformly over the simplex S_m computing the corresponding classwise (FPR, TPR) pairs. The resulting point sets form the *ROC clouds*, which represent all achievable operating points under a single, coherent multiclass decision rule. Unlike standard One-vs-Rest (OvR) curves, which vary independent thresholds per class, the ROC clouds reflect realistic joint trade-offs among classes. For reference, the orange curves in the figures show the traditional OvR ROC curves. These are computed as follows: for each class j , scores \hat{y}^j are compared against a binarized label (j vs. rest) and the threshold on \hat{y}^j is swept to trace (FPR, TPR).

Typically, the ROC clouds lie below or on par with the OvR curves, as expected since the latter represent the best possible performance when varying thresholds independently per class. Nevertheless, as seen in the SOLAR-STORM1 case especially for class beta, points in the cloud can exceed the OvR curve, showing that the simplex-based rule provides better performance compared to argmax, as confirmed also by the result in 3. Instead, in the OCTMNIST case, the same table shows that the simplex decision rule does not give an edge in the test scores, and consequently the ROC clouds are mostly below or on par with the OvR curves.

The DFP computations for these datasets are summarized in 5 and quantify the visual gaps in the clouds: in SOLAR-STORM1, *beta* (0.2297) is closest to $(0, 1)$ while *alpha* (0.3312) is farthest; in OCTMNIST, *Drusen* (0.2264) and *Normal* (0.2262) are most separable, whereas *CNV* (0.3042) is most challenging.

Dataset	Class 1	Class 2	Class 3	Class 4	Overall DFP
SOLAR-STORM1	0.3312	0.2297	0.2471	—	0.2693
OCTMNIST	0.3042	0.2735	0.2264	0.2262	0.2576

Table 5: Per-class and overall DFP values for SOLAR-STORM1 and OCTMNIST. Smaller DFP values correspond to ROC clouds closer to the ideal top-left corner $(0, 1)$, indicating better class separability.

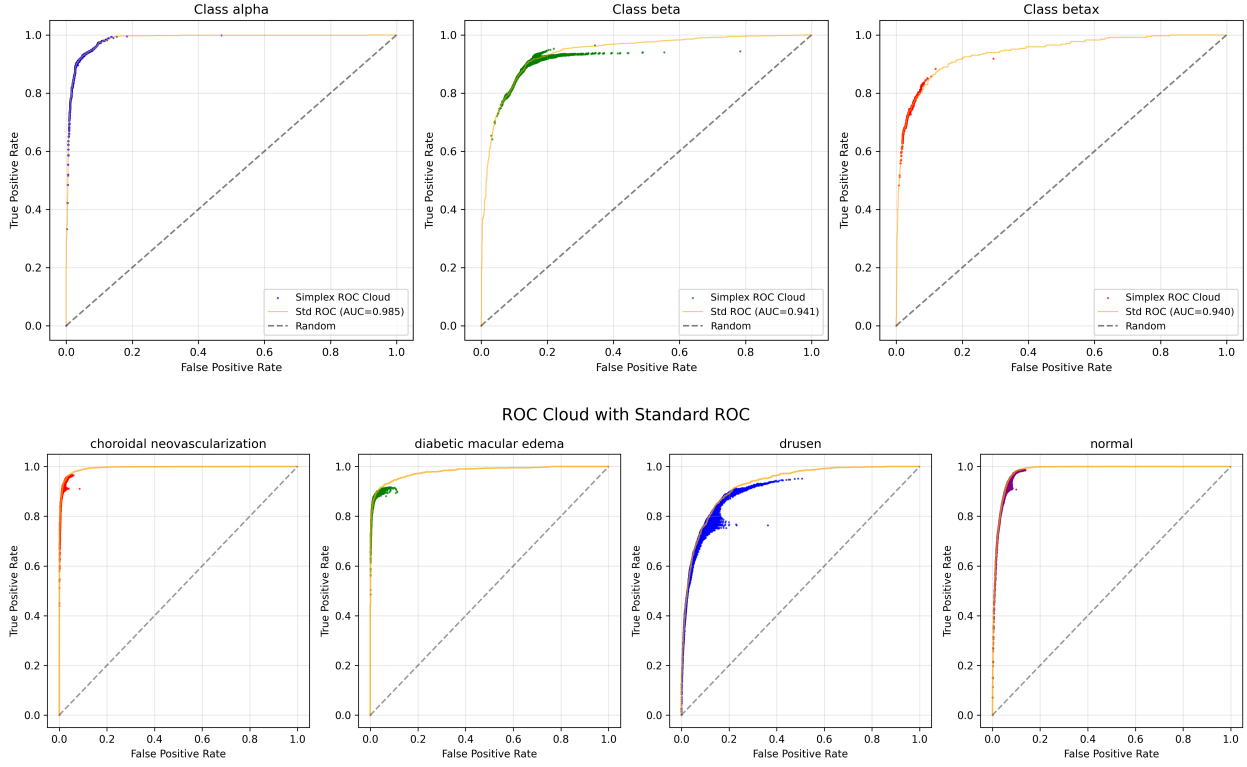


Figure 4: ROC clouds with OvR ROC curves (orange). Top: SOLAR-STORM1. Bottom: OCTMNIST (validation set).

6 Discussion

The experiments carried out in 5.1 show the effectiveness of the proposed threshold tuning approach in enhancing and improving the performance of classification networks. As it can be applied a posteriori to any neural classifier, this procedure has the potential to become a common practice, just as classical one-dimensional threshold tuning in a binary setting. As intuition suggests from the binary case, such multidimensional threshold tuning could be especially meaningful in unbalanced settings. Note that in 3 the best threshold turns out to be *close* to the minority class, as one would expect in a binary task.

We remark that the effectiveness of tuning the threshold on the validation set to improve the performance on the test set is strongly influenced by the classes' distribution. Indeed, even if, according to machine learning theory, validation and test sets should be characterized by an analogous classes' distribution [29], this may not take place in fact, thus determining a calibration discrepancy between validation and test sets. In our tests reported in 3, we actually obtained the worst result, i.e., a worse performance on the test set with respect to the argmax rule, in the case where the classes' distribution on the test set deviates the most from the validation one, that is the case of the OCTMNIST dataset. Besides reasonable oscillations in performance due to random factors, initializations, and train/test splits, differences between validation and test compositions are usually responsible for unsatisfactory calibration results.

Furthermore, we compared the performance of our proposed tuning strategies with respect to other state-of-the-art decision rules. Results in 4 demonstrate the effectiveness of the Tuned threshold approach, which consistently matches or exceeds the performance of both the baseline

argmax and the alternative decision rules.

A principal advantage of the Tuned strategy is that, by design, it can only improve upon or equate the performance of the classical *argmax* rule on the validation set. This is because the *argmax* condition corresponds to the barycenter of the simplex, which is one of the candidate thresholds evaluated during the tuning process. In contrast, other competitive strategies, such as the Fréchet mean or the ε -inflated *argmax*, may yield occasional performance degradation compared to the standard procedure. As is standard, the generalization of performance to the test set depends on factors such as the congruence of class distributions between the validation and test splits. Regarding the ε -inflated *argmax*, while its “Coverage” score is sometimes marginally higher than that of Tuned and other methods, this is attributable to its set-based prediction mechanism. When restricted to single-label outputs (“Singleton” accuracy), the ε -inflated *argmax* generally underperforms compared to Tuned. These findings underscore the robustness and practical significance of the proposed Tuned threshold framework.

As far as the proposed ROC analysis is concerned, 4 visualizes the proposed ROC clouds alongside the standard OvR curves. As expected, clouds typically lie below or on par with OvR, because OvR sweeps an unconstrained per-class threshold and thus traces an idealized, class-isolated frontier for the considered class while ignoring the consequences for the others. In contrast, each point in a ROC cloud is produced by a *single* multiclass threshold τ applied to all classes simultaneously, mapping the realistic, system-wide trade-offs enforced by a coherent decision rule. It follows that the ROC cloud maps out the true, constrained performance envelope of the classifier in a multiclass setting.

In addition, the simplex decision rule is more nuanced than the simple thresholding of the OvR approach: it defines decision regions not with a simple cut, but with relational hyperplanes within the simplex. This allows for a more detailed exploration of the trade-offs between classes. In cases where the optimal decision boundary is relational (e.g., “predict class A when its probability is high, especially if class B’s is low”), this finer rule can discover efficiencies that the simpler OvR method cannot. This is why, for certain data distributions, operating points from the simplex method can locally exceed the standard ROC curve (see top row of 4).

Finally, we introduce the DFP metric to summarize the distribution of the ROC points and get a measure of class separability.

7 Conclusions

We introduced a threshold-based framework for multiclass classification that treats softmax outputs as points on the simplex and replaces the standard *argmax* with a multidimensional threshold. This yields an inference-time decision rule that requires no retraining or post-hoc calibrators and supports *a posteriori* optimization of any macro-aggregated score directly on validation data. Across several networks and datasets, we have seen from experiments that multidimensional threshold tuning can improve upon the *argmax* baseline, with the largest gains appearing in unbalanced settings.

Also, we introduced *ROC clouds* based on the simplex decision rule. These consist of the attainable (FPR, TPR) operating points found by varying thresholds across the multidimensional simplex. In contrast to standard One-vs-Rest ROC curves, which sweep class-wise thresholds independently and thus trace an idealized class-isolated frontier, the ROC clouds capture the joint trade-offs enforced by one single natively multiclass decision rule. We further summarized each cloud with the *Distance From Point* (DFP), the mean L_1 distance to $(0, 1)$.

Finally, we point out that while multidimensional threshold tuning is clearly fully parallelizable, the optimization procedure becomes expensive if *many* classes are involved due to the curse of

dimensionality. In order to overcome this issue, one may look for the optimal threshold on a more *rough* discretization of the simplex, sampling a fixed number of threshold values by means of a Monte Carlo approach or exploring the threshold space by means of suitable parameter searches (e.g., Bayesian schemes).

Acknowledgments

E.L. was supported by the HORIZON Europe ARCAFF Project, Grant No. 101082164. All authors acknowledge the Gruppo Nazionale per il Calcolo Scientifico - Istituto Nazionale di Alta Matematica (GNCS - INdAM).

References

- [1] Erin L Allwein, Robert E Schapire, and Yoram Singer. Reducing multiclass to binary: A unifying approach for margin classifiers. *Journal of machine learning research*, 1(Dec):113–141, 2000.
- [2] Andrew P Bradley. The use of the area under the roc curve in the evaluation of machine learning algorithms. *Pattern recognition*, 30(7):1145–1159, 1997.
- [3] John S Bridle. Probabilistic interpretation of feedforward classification network outputs, with relationships to statistical pattern recognition. In *Neurocomputing: Algorithms, architectures and applications*, pages 227–236. Springer, 1990.
- [4] Yuanhui Fang, Yanmei Cui, and Xianzhi Ao. Deep learning for automatic recognition of magnetic type in sunspot groups. *Advances in Astronomy*, 2019(1):9196234, 2019.
- [5] Tom Fawcett. An introduction to roc analysis. *Pattern recognition letters*, 27(8):861–874, 2006.
- [6] César Ferri, José Hernández-Orallo, and Miguel Angel Salido. Volume under the roc surface for multi-class problems. In *European conference on machine learning*, pages 108–120. Springer, 2003.
- [7] Ian Goodfellow, Yoshua Bengio, and Aaron Courville. *Deep learning*. Adaptive Computation and Machine Learning. MIT Press, Cambridge, MA, 2016.
- [8] Sabrina Guastavino, Francesco Marchetti, Federico Benvenuto, Cristina Campi, and Michele Piana. Implementation paradigm for supervised flare forecasting studies: A deep learning application with video data. *Astronomy & Astrophysics*, 662:A105, 2022.
- [9] Chuan Guo, Geoff Pleiss, Yu Sun, and Kilian Q Weinberger. On calibration of modern neural networks. In *International conference on machine learning*, pages 1321–1330. PMLR, 2017.
- [10] David J Hand and Robert J Till. A simple generalisation of the area under the roc curve for multiple class classification problems. *Machine learning*, 45(2):171–186, 2001.
- [11] David Harris and Sarah Harris. *Digital Design and Computer Architecture, Second Edition*. Morgan Kaufmann Publishers Inc., San Francisco, CA, USA, 2nd edition, 2012.
- [12] Raoul Heese, Jochen Schmid, Michał Walczak, and Michael Bortz. Calibrated simplex-mapping classification. *PLoS One*, 18(1):e0279876, 2023.

[13] Geoffrey Holmes, Bernhard Pfahringer, Richard Kirkby, Eibe Frank, and Mark Hall. Multi-class alternating decision trees. In *European Conference on Machine Learning*, pages 161–172. Springer, 2002.

[14] Jakob Nikolas Kather, Johannes Krisam, et al. Predicting survival from colorectal cancer histology slides using deep learning: A retrospective multicenter study. *PLoS Medicine*, 16(1):1–22, 01 2019.

[15] Daniel S. Kermany, Michael Goldbaum, et al. Identifying medical diagnoses and treatable diseases by image-based deep learning. *Cell*, 172(5):1122 – 1131.e9, 2018.

[16] Ross Kleiman and David Page. Auc μ : A performance metric for multi-class machine learning models. In *International Conference on Machine Learning*, pages 3439–3447. PMLR, 2019.

[17] Thomas CW Landgrebe and Robert PW Duin. Efficient multiclass roc approximation by decomposition via confusion matrix perturbation analysis. *IEEE transactions on pattern analysis and machine intelligence*, 30(5):810–822, 2008.

[18] Edoardo Legnaro, Sabrina Guastavino, Michele Piana, and Anna Maria Massone. Deep learning for active region classification: A systematic study from convolutional neural networks to vision transformers. *The Astrophysical Journal*, 981(2):157, 2025.

[19] F. Marchetti, S. Guastavino, M. Piana, and C. Campi. Score-Oriented Loss (SOL) functions. *Pattern Recognition*, 132:108913, 2022.

[20] Andre Martins and Ramon Astudillo. From softmax to sparsemax: A sparse model of attention and multi-label classification. In *International conference on machine learning*, pages 1614–1623. PMLR, 2016.

[21] Youssef Mroueh, Tomaso Poggio, Lorenzo Rosasco, and Jean-Jacques Slotine. Multiclass learning with simplex coding. *Advances in Neural Information Processing Systems*, 25, 2012.

[22] Kevin P Murphy. Machine learning: A probabilistic perspective (adaptive computation and machine learning series). *The MIT Press: London, UK*, 2018.

[23] WD Pesnell, BJ Thompson, and PC Chamberlin. *The solar dynamics observatory (SDO)*. Springer, 2012.

[24] Nicholas Roberts, Xintong Li, Dyah Adila, Sonia Cromp, Tzu-Heng Huang, Jitian Zhao, and Frederic Sala. Geometry-aware adaptation for pretrained models. *Advances in Neural Information Processing Systems*, 36:49628–49658, 2023.

[25] Philip Hanby Scherrer, Jesper Schou, RI Bush, AG Kosovichev, RS Bogart, JT Hoeksema, Y Liu, TL Duvall, J Zhao, AM Title, et al. The helioseismic and magnetic imager (hmi) investigation for the solar dynamics observatory (sdo). *Solar Physics*, 275:207–227, 2012.

[26] Jake Soloff, Rina Barber, and Rebecca Willett. Building a stable classifier with the inflated argmax. *Advances in Neural Information Processing Systems*, 37:70349–70380, 2024.

[27] Long Tang, Yingjie Tian, and Panos M Pardalos. A novel perspective on multiclass classification: Regular simplex support vector machine. *Information Sciences*, 480:324–338, 2019.

- [28] Hugo Touvron, Matthieu Cord, Matthijs Douze, Francisco Massa, Alexandre Sablayrolles, and Hervé Jégou. Training data-efficient image transformers & distillation through attention. In *International conference on machine learning*, pages 10347–10357. PMLR, 2021.
- [29] Vladimir N. Vapnik. *Statistical Learning Theory*. Wiley-Interscience, 1998.
- [30] Matthew S Wandishin and Steven J Mullen. Multiclass roc analysis. *Weather and Forecasting*, 24(2):530–547, 2009.
- [31] Ross Wightman. Pytorch image models. <https://github.com/huggingface/pytorch-image-models>, 2019.
- [32] Han Xiao, Kashif Rasul, and Roland Vollgraf. Fashion-mnist: a novel image dataset for benchmarking machine learning algorithms. *arXiv preprint arXiv:1708.07747*, 2017.
- [33] Jiancheng Yang, Rui Shi, and Bingbing Ni. Medmnist classification decathlon: A lightweight automl benchmark for medical image analysis. In *IEEE 18th International Symposium on Biomedical Imaging (ISBI)*, pages 191–195, 2021.
- [34] Jiancheng Yang, Rui Shi, Donglai Wei, Zequan Liu, Lin Zhao, Bilian Ke, Hanspeter Pfister, and Bingbing Ni. Medmnist v2-a large-scale lightweight benchmark for 2d and 3d biomedical image classification. *Scientific Data*, 10(1):41, 2023.
- [35] Bianca Zadrozny and Charles Elkan. Transforming classifier scores into accurate multiclass probability estimates. In *Proceedings of the eighth ACM SIGKDD international conference on Knowledge discovery and data mining*, pages 694–699, 2002.
- [36] G.P. Zhang. Neural networks for classification: a survey. *IEEE Transactions on Systems, Man, and Cybernetics, Part C (Applications and Reviews)*, 30(4):451–462, 2000.